Part A: English Edition

Journal of Textiles and Polymers

Vol. 10, No. 3, 23-34, July 2022

ORIGINAL PAPER

Effect of APTES-Halloysite Nanotubes on the Release Characteristic of Cellulose Acetate/Curcumin Film

Elnaz Salarian[1], Atefeh Solouk[2], and Somaye Akbari[3*]

Received: 13 April 2022, Accepted: 17 October 2022

***Abstract*- In this research, the fabrication of nanocomposite films consisting of cellulose acetate (CA), pristine and modified halloysite nanotubes (mHNTs), and curcumin was investigated by solution casting method for wound dressing applications. The chemical structure, morphology, and surface properties of the samples were studied by Fourier transform infrared (FTIR) spectroscopy, scanning electron microscopy (SEM), and contact angle measurement. Furthermore, the effects of modified halloysite nanotube were examined on mechanical properties, water vapor transmission rate (WVTR), and curcumin release. The results revealed that mHNTs enhanced mechanical strength and hydrophilicity, as well as it increased curcumin release, and controlled its release rate, which this could be attributed to the high activity of terminal groups (amine) comparing to pristine halloysite nanotubes (HNTs). Moreover, better adhesion and integrity between the nanoparticles and polymeric matrix were confirmed by enhancement in mechanical strength. The cell proliferation assay also indicated the biocompatibility and nontoxicity of the samples and their potential of being an appropriate substrate for cell adhesion.**

***Keywords*: cellulose acetate, halloysite nanotubes, curcumin, wound dressing, modification**

E. Salarian
Biomedical Engineering Department, Islamic Azad University, Central Tehran Branch, Tehran, Iran.

A. Solouk
Biomedical Engineering Department, Amirkabir University of Technology (Tehran Polytechnic), Tehran, Iran.

S. Akbari
Textile Engineering Department, Amirkabir University of Technology (Tehran Polytechnic), Tehran, Iran.

Correspondence should be addresses to S. Akbari
e-mail: akbari_s@aut.ac.ir

I. INTRODUCTION

Cellulose acetate (CA) is one of the most usual biopolymers in the world and primitive ingredient of the cell wall of green plants. CA is acetate ester of cellulose and its most significant derivative in the commercial. It is produced by the reaction of acetic anhydride with cellulose while, sulfuric acid acts as the catalyst in this reaction. The degree of polymerization and the number of acetyl group for each glucose unit change CA properties [1]. CA is broadly applicable in many fields, namely tissue engineering [2,3], wound dressing [4-6], and drug delivery systems [7-9].

Wound infections occur when microorganisms invade damaged tissue. Bacteria from skin or outside environment are the most crucial factor in causing wound infections. Normal flora of bacteria exists in the skin which is innocuous. After skin injury, protective layer of skin will be destroyed and the normal flora will colonize the injured part. It leads to tissue injury and inflammation, therefore causing severe complications [10].

Using biocompatible scaffold combined with antibacterial agents is a treatment approach for injured tissue [11]. Curcumin with a polyphenol structure produced by some plants is one of the natural antibacterial agents with various characteristics. It has multiple pharmacological and biological actions, such as anti-apoptosis [12-14], anti-proliferation [15,16], anti-angiogenesis [17], anti-inflammatory [18], antitumor [19,20], antioxidant [21,22], and antibacterial [23] which make it popular. Sidhu *et al*. [24] have investigated the effect of curcumin therapy on wound healing. For animals wounds, curcumin causes early re-epithelialization, better neovascularization, enhanced migration of different cells into the wound, and more collagen content in healed skin [25].

Anyway, there are some impediments with the bioavailability of curcumin, notably after oral or topical application. Curcumin hydrophobicity, rapid degradation of that under neutral or non-acidic conditions, and its short half-life are serious impediments [26]. Accordingly, a suitable carrier could comfort curcumin delivery and increase its pharmaceutical uses. Nanoscale carriers such as clay minerals are promising candidates because of their superior properties such as excellent mechanical durability, large specific surface area, and high biocompatibility [27]. Among clay minerals, HNTs have attracted much attention due to their full availability and physicochemical properties namely tubular morphology, high porosity, high receptor surface chemistry and hydrophobicity [28].

Chiara *et al*. proved high efficiency of HNTs as nano-carriers in naked and coated forms [29]. Nanocomposites containing HNTs have been used extensively due to their antibacterial, catalytic, optical, electrical, and magnetic characteristics. HNTs were loaded with gentamicin and employed as fortifying materials for the bone implant with polymethyl methacrylate (PMMA) matrix, resulting in enhanced mechanical and physical properties of PMMA [30].

Nowadays, surface treatments are an issue of great concern because it makes a material better in some way. The high porosity of internal structure of HNTs makes their functionalization treatments so much easier. It is the most significant advantage of HNTs over other minerals like bentonite. Different approaches have been taken to functionalize HNTs such as HNTs-octadecylphosphonic [31], HNTs-chitosan [32,33], HNTs-lactic acid [34], HNTs-HDTMA (hexadecyltrimethylammonium) [35], and HNTs-APTES [36,37]. An appropriate method to enhance the number of hydrophilic groups on HNTs surfaces is grafting amine groups. For example, (3-aminopropyl) triethoxysilane (APTES) can be utilized to provide amine group functionalized HNTs [38,39]. APTES makes a profound contribution in strengthening the interfacial interaction between matrix and HNTs [40,41].

In this study, curcumin was dispersed in CA solution to induce antibacterial properties in CA matrix. Furthermore, mHNTs were selected as curcumin carriers, and the samples were fabricated by solution casting. The Fourier-transform infrared (FTIR) spectroscopy, scanning electron microscopy (SEM), and contact angle measurement were employed for investigating the chemical structure, morphology, and surface properties of the samples, respectively. Mechanical properties, water vapor transmission rate (WVTR), and drug release of the halloysite-containing and halloysite-free samples were then studied. Cell adhesion, cell proliferation, as well as the antimicrobial activity of the samples were analyzed.

II. EXPERIMENTAL

A. Materials

Cellulose acetate (mw 30 kDa) and N,N-dimethylformamide (DMF) were purchased from Sigma–Aldrich Company and used as received. Sodium bicarbonate and glutaraldehyde 25 wt% were supplied by Merck Company. The HNTs (80 nm diameter) were kindly donated by Delta-Dolsk Company, Poland. Aminepropyltriethoxysilane (APTES) and curcumin (Cur) as active antibacterial and antiinflammatory materials were purchased from Sigma-Aldrich Company, Germany. Methanol, acetone, and all the other chemicals were of laboratory reagent grade and supplied by Sigma-Aldrich. The results revealed that mHNTs enhanced mechanical strength and hydrophilicity, increased curcumin release, and also controlled its release rate due to the high activity of terminal groups (amine) comparing to pristine halloysite nanotubes (HNTs).

B. Halloysite Modification and Preparation of CA, CA/Cur, and CA/mHNTs/Cur Films

The steps mentioned below are taken for preparing amine group functionalized HNTs. Firstly, a distribution of HNTs in HCl 35 wt% was prepared and stirred for 24 h at room temperature. After that, as-prepared distribution was washed with distilled water to have a practically constant pH value after third washing. After purification, HNTs were collected on a neat substrate and placed in an oven at 60 °C for 24 h. A mixture of HNTs (30 g), toluene (150 mL), and APTES (40 mL) was heated under reflux at 60 °C for 12 h for the introduction of amino groups into HNTs. Then, the resultant solution was repeatedly washed with diethyl ether, ethanol, and methanol for the complete elimination of impurities and dried at 60 °C [32].

In order to prepare CA film, 5 w/v% CA was dissolved in 5 v/v% acetone/DMF solution at room temperature and stirred for 24 h. The solution was poured in a glass petri dish and dried in a vacuum oven at 40 °C for 24 h. Finally, the CA films were separated from petri dishes and before any test implementation, incubated in a desiccator at room temperature for 24 h. For fabrication of CA-containing curcumin (CA/Cur) film, 5 w/v% CA was dissolved in 5 v/v% acetone/DMF solution at room temperature. Then, curcumin was added to the solution and stirred for 24 h at 80 °C. Curcumin to CA mass ratio was about 1:10 in this solution. Subsequent steps were the same as the preparation steps of polymeric CA film. For preparing cellulose acetate/modified halloysite nanotubes/curcumin (CA/mHNTs/Cur) film, first, we dispersed 0.24 g of halloysite in 20 mL of water for one hour at a temperature of 80 °C. Then, we dissolved 0.023 g of curcumin in 5 mL of methanol and placed

it at 80 °C for two hours and then centrifuged for 24 h at 50 °C, and again 5 w/v% CA was dissolved in 5 v/v% acetone/DMF solution at room temperature. Afterward, halloysite (halloysite:CA mass ratio was about 1:10) was added to the solution and stirred at room temperature for 24 h. The solution was poured in a petri dish and dried at 40 °C for 24 h. Subsequent steps were the same as the preparation steps of polymeric CA film.

C. Characterization

C.1. Water Uptake Test

For wound-healing process, one of the most important criteria for keeping a moist environment is water uptake of dressing. To achieve this goal, the petri dishes containing different samples were embedded in PBS solution at 27 °C. Eight samples were measured at equal time intervals, and it lasts for 12 h. Eventually, samples weight changes were recorded and used to calculate water uptake percentage by using Eq. (1) [42], where m_w and m_d are the weight of samples in wet and dry conditions, respectively:

$$\text{Water uptake } (\%) = \frac{m_w - m_d}{m_d} \quad (1)$$

D. Contact Angle Measurement

For determining hydrophilicity, static contact angles were investigated using a Rruss Glo device, and 10 µL of samples were used for each point. When a water drop is distilled on a sample, the liquid will expand like a thin film or spread limitedly as a drop on the sample. In order to compensate the sample movements from the horizontal line during the preparation process, the contact angle was calculated as the average of 5 measurements.

E. Water Vapor Transmission Rate (WVTR) Test

The moisture permeability of the films was determined using the water vapor transmission rate (WVTR) calculation. Each sample was cut into a disc with an approximate diameter of 1.5 cm and mounted on the mouth of a cylindrical glass cup containing DI water with a diameter of 1.3 cm. In order to prevent any water vapor loss through the boundaries, the samples were sealed using glue across the edges and then placed in a dry at 27 °C. The assembly was weighed at regular time intervals. Then, a graph of the amount of weight loss versus time was plotted. From the slope of the graph, WVTR was measured by using Eq. (2), where S is the slope of weight changing-time graph, and A is the area of the glass:

$$\text{WVTR}\left(\frac{g}{m^2 \times day}\right) = \frac{(S \times 24)}{A} \quad (2)$$

F. FTIR Analysis

Fourier-transform infrared (FTIR) spectra were recorded over the range of 4000-500 cm^{-1} on an Avatar 360 (Thermo Nicolet, Waltham, MA) spectrometer.

G. SEM Analysis

Morphology of samples was investigated using a Cambridge S-360 scanning electron microscopy (SEM) at an accelerating voltage of 10 kV. All samples were gold-coated by a polaron sputter coater before SEM analysis.

H. Stress-Strain Test

The mechanical properties of the substitutes were determined using a stress-strain test machine (Instron 5565, UK, and Santam STM-20, Iran). In brief, a uniform area of 4 cm×1.5 cm of the three samples of films was mounted lengthwise between the two grips of the machine. Semi-thickness skin samples were subjected to load cell of 50 N with 1mm/min strain rate in Instron device, while fascia and acellular dermis samples were subjected to load cell of 200 N. During the procedure, to ensure minimization of sample deformation, the force was stayed parallel to the stretching direction. The fracture of the samples and changes in load-bearing were recorded. Then, elasticity modulus, strain strength, stress-at-break point, and strain-at-break point were calculated.

I. In Vitro Cell Culture

For *in vitro* cell culture, rabbit and human chondrocytes were grown in DMEM/F12 including 10% FCS, 100 U/mL penicillin, and 100 µg/mL streptomycin. These cells were cultured on the surface of the samples, and they were kept in a damp environment at 37 °C with 5% CO_2 for 14 days [43].

J. In Vitro Curcumin Release

A novel approach, which has already been performed, was used for evaluation of in vitro drug release. 0.5 g of the drug-loaded halloysite samples was immersed in 100 mL of the phosphate buffer solution (PBS, pH=7.4). The resulted mixture was stirred at 37 °C and used as a dissolution apparatus. Within the chosen time intervals, 4 mL of the solution was removed, and 4 mL PBS solution was added back to compensate volume changes. For minimizing the drug release of remaining drug-loaded halloysite, the solution was centrifuged after removing samples.

The amount of drug release was studied by UV absorption via a single beam device and absorption was compared by a ranking function. According to the standard diagram of curcumin release and regarding obtained intensities, concentrations were calculated and put in Eq. (3) [44].

After calculating required concentrations, drug release percentage was obtained by dividing final concentration to loaded drug concentration and multiplying by 100.

$$C_n^1 = C_n\left(\frac{V_T}{V_T - V_S}\right)\left(\frac{C_{n-1}^1}{C_{n-1}}\right) \quad (3)$$

K. Weight Loss Analysis

For weight loss analysis, rectangular cuboids with dimensions 3×5×4 mm^3 were cut from films. The samples were incubated in PBS solution at 37 °C, and their weights were gauged. Then, the samples were washed and freeze-dried for 10 h, and their weight loss percentages were computed at each incubation time. Calculations were performed by using Eq. (4), where W_0 and W_f are the first and final weights of the samples [2]:

$$\text{Weight loss } (\%) = \frac{(w_o - w_f)}{w_o} \quad (4)$$

L. MTT Assay

The cytotoxicity of the samples was investigated based on a method extracted from the ISO 10993-5 standard test method (indirect contact). The reduction of the tetrazolium component of MTT by viable cells was measured by this test. Thus, the level of the reduction of MTT into formazan is an indicator of the level of cell metabolism. For the MTT assay, the samples were sterilized and incubated at 37 °C for 1 and 5 days with an extraction ratio of 6 $cm^2.mL^{-1}$.

In brief, 1×10^4 cells and 100 µL culture medium were added to each well of a 96-well microtiter plate and incubated for 24 h. Thereafter, the culture medium of each well was replaced with the above-mentioned extraction medium and incubated for another 24 h. MTT solution was poured into the medium above the samples followed by incubation at 37 °C for 4 h. Afterward, the formed formazan crystals were dissolved in the MTT solvent, and the optical density was determined by a spectrophotometer at 570 nm. The average optical density of control and other samples was put in Eq. (5) to obtain the relative cell viability or cell growth (%) normalized by the control group [45,46].

$$\text{Cell viability } (\%) = \frac{\text{average optical density of samples}}{\text{average optical density of control}} \times 100 \quad (5)$$

M. Cell Seeding on the Samples

Adipose-derived stem cells were isolated from adipose tissue of human prepared by Department of the Biotechnology, University of Tehran. The cells were then seeded on the sterilized samples at the density of 2×10^4 (20000-30000 fibroblast cell L929) per well in Dulbecco's modified Eagle's medium (Invitrogen, USA) supplemented with 10% fetal bovine serum (Invitrogen, USA), incubated at 37 °C with 5% CO_2.

N. Characteristic of Cell Morphology with SEM

After 1 day of cell seeding, the samples were washed twice at PBS and then stabilized with 2.5% glutaraldehyde at 4 °C for 2 h. Then, the samples were air-dried under a hood and gold-coated and then imaged by SEM.

O. Statistical Analysis

Statistical analysis was carried out using analysis of variance. Mean standard deviation was calculated by data obtained from triplicate samples (n=3) and was considered statistically significant when $P<0.05$.

P. Antibacterial Test

Antibacterial test shows the efficiency of samples in killing gram-negative and gram-positive bacteria. For this purpose, the antibacterial activities of films were investigated against model microbial species, including *Escherichia coli* (gram-negative) and *Staphylococcus aureus* (gram-positive), according to the clinical and laboratory standards institute (CLSI) using the method of 0.5 McFarland standard. The films were cut into 6 mm diameter discs and placed on Mueller-Hinton agar plates (QUELAB, UK) inoculated with bacteria's [47,48]. After 24 h of incubation at 37 °C, the inhibited areas of bacterial growth were measured by Image J software.

III. RESULTS AND DISCUSSION

A. Water Uptake

Figs. 1 and 2 show the absorption percentage of CA, CA/Cur, and CA/mHNTs/Cur films after 24 and 48 h of immersion, respectively. CA/mHNTs/Cur film is inflated

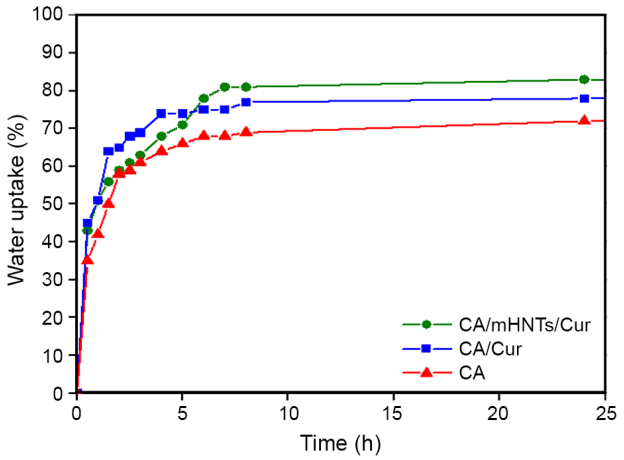

Fig. 1. Water uptake versus time for CA, CA/Cur, and CA/mHNTs/Cur films.

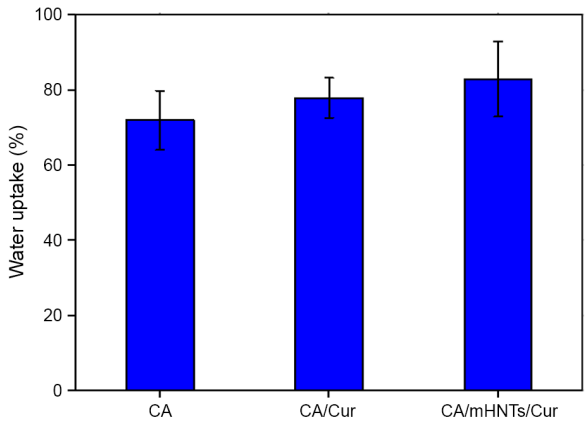

Fig. 2. Column graph for water uptake of CA, CA/Cur, and CA/mHNTs/Cur films at 48 h.

about 83% of its primary weight in PBS solution. Indeed, after 24 h, the absorption of CA/mHNTs/Cur film is more than that of CA and CA/Cur films. It is due to the numerous terminal groups (amine) of modified halloysite, keeping curcumin for longer times. So, before primary 24 h, there is less curcumin in comparison to CA and CA/Cur samples. After a while, curcumin adhesion to halloysite walls will decrease, and it absorbs more PBS to itself.

According to the statistical analysis, the correlation or significance coefficient between CA and CA/Cur is 0.00987 and between CA and CA/HNT/Cur is 0.00883. Also, the correlation coefficient between CA/Cur and CA/HNT/Cur is 0.00845 and the correlation coefficient between 3 variables is 0.00962. The results reveal that the high distribution of data is due to many changes in different hours. In this way, this amount increases during different hours and it has increased with a suitable slope during a relatively long period (Fig. 1). As shown in Fig. 2, there is no significant difference between the variables ($P>0.05$). The results show that the Mean±SD scores are at an almost appropriate level and the confidence level is 95%.

B. Contact Angle

Contact angle test is a good determinant for film hydrophilicity, and when it is less than 90°, the corresponding film is hydrophilic. This test is repeated five times, and an average is reported. The surface contact angles of CA, CA/Cur, CA/mHNTs/Cur films are investigated. As shown in Fig. 3, the amount of hydrophilicity and contact angle changes when the drug and/or halloysite are added. Contact angle decreases and hydrophilicity increases, also activating halloysite operating groups have the same effect. The contact angle of CA/Cur enhanced owing to the chemical structure of curcumin. Moreover, Water and air transmission improved due to the tubular structure of halloysite.

According to the statistical analysis, the coefficient of significance between the variable CA and CA/Cur and CA/HNT/Cur is 0.04995 and the coefficient of significance between CA/Cur and CA/HNT/Cur is 0.842; finally, the overall significance coefficient is 0.79. The standard deviation of the data is a little high compared to their mean, which indicates the distribution of the data. According to Fig. 3, there is a significant relationship between only two series of variables. There is a significant relationship between the polymer film of CA and CA/Cur, and then between CA and CA/HNT/Cur. By means of SPSS software, the data are verified with each other and the relationship between the data is measured. There is a significant relationship between only two series of variables. The results of this test show that the data have a high level of distribution and diminish the reliability of the data.

C. Water Vapor Transmission Rate (WVTR)

The steam permeability of the film was measured in every hour in periods of 7, 24, and 48 h. The rate of permeability was calculated in permanent dynamic mode. Therefore, the water absorbed by the film was neglected. Water removed

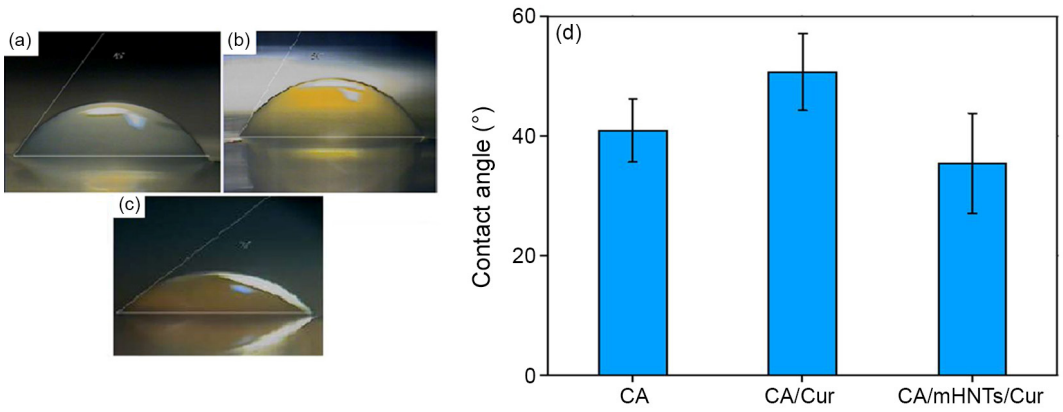

Fig. 3. Contact angle of: (a) CA, (b) CA/Cur, (c) CA/mHNTs/Cur films (left), and (d) Column graph for contact angle of the samples.

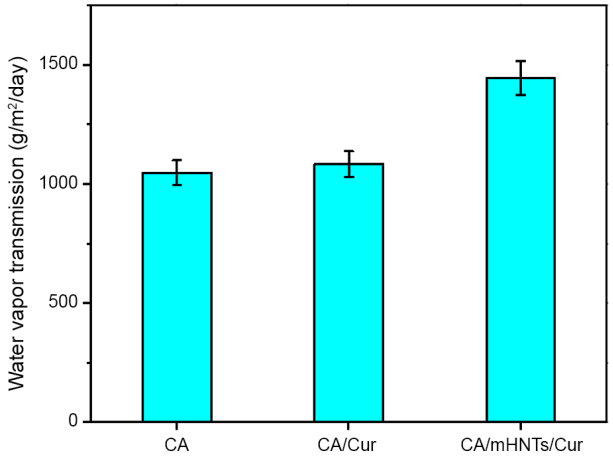

Fig. 4. Column graph for the water vapor transmission rate of CA, CA/Cur, and CA/mHNTs/Cur films.

from the system by evaporation as it passes through the film is linearly dependent on time ($R^2 \geq 0.99$), implying a constant rate for steam passage.

The results of the WVTR tests were obtained for CA, CA/Cur, and CA/mHNTs/Cur films. According to Fig. 4, there is a significant difference between CA/mHNTs/Cur and two other films. It is evident from the results that WVTR of CA/mHNTs/Cur film increased in comparison with CA film. Also, the water vapor transmission rate in CA/mHNTs/Cur film is more than that in CA/Cur film. It can be said that the addition of halloysite with the mentioned properties will facilitate the transmission of water and air and, in the same way, the WVTR.

According to Fig. 4, there is a significance level of 0.01 between CA/HNT/Cur composite film and other two samples. The results show that the Mean±SD scores are at an almost appropriate level and the confidence level is 95%.

D. FTIR Spectroscopy

The chemical structure of curcumin, halloysite, cellulose acetate, CA film, CA/Cur, and CA/mHNTs/Cur samples was analyzed by FTIR test (Fig. 5). There are new peaks in the FTIR spectra of CA/Cur that indicates the placement of curcumin in the polymer film. For example, the alcohol peak of CA is sharp, but the phenol peak of curcumin is slightly broad. So, the overlap of these two peaks gave rise to a smooth broad peak at 3461 cm^{-1} in CA/Cur.

Curcumin has carbonyl groups created from a carbon atom double-bonded to an oxygen atom. For CA/Cur, the typical carbonyl peak is replaced by peaks at 1733 and 1654 cm^{-1} corresponding to single-bonded carbon and oxygen atom. In addition to the negative shift, the intensity and height of the peak decreased. The increase in the intensity and width of the peak at 1733, 1300, and 1400 cm^{-1} indicates the increase in the concentration of C=O and

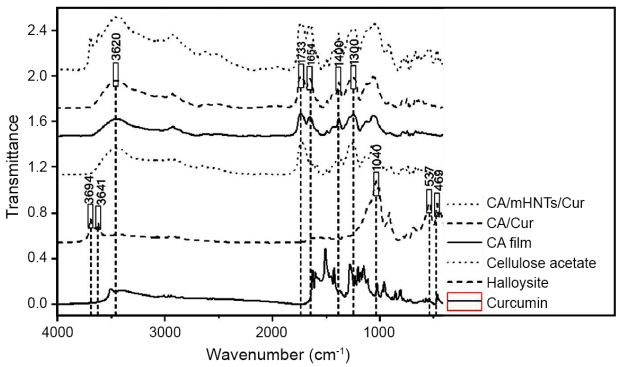

Fig. 5. FTIR spectra of curcumin, halloysite, cellulose acetate, CA film, CA/Cur, and CA/mHNTs/Cur samples.

C-O, which shows the presence of CA and curcumin in the film. This study, which is consistent with that of Owlia *et al*., concluded that the halloysite peaks that reveal the presence of halloysite in polymer films are O-H band at 3620-3694 cm^{-1}, Si-O-Si bending band at 469 cm^{-1}, Al-O-Si strain band at 537 cm^{-1}, and Si-O-Si bending band as a widened peak at 1067 cm^{-1}. They prove that Si is present in polymer films [49].

For CA/mHNTs/Cur film, the peaks at 3694 and 3620 cm^{-1} (twin peaks appeared) are related to OH strain vibrations on the surface of halloysite. The Si-O-Si bond vibrations at 1040-1067 cm^{-1} are fully sharped, which indicate the existence of halloysite.

E. SEM

According to the SEM images of samples shown in Fig. 6, CA film has a relatively flat surface. After taking the drug, the morphology changes because curcumin appears as micelle on the polymeric surface. Also, adding halloysite changes surface morphology of the CA polymeric film. Halloysite cylinders as suitable substrates for drug loading have curcumin in the internal and external wall. Curcumin migrates to the surface and increases contact angle and forms cavities on the surface. Theses phenomenon lead to faster degradation and easier release of curcumin.

F. Stress-Strain Test

The thickness of the films was measured at different points, and its average value was obtained 250-300 µm. According to the tensile results taken from the stretcher device, the stress-strain curves were plotted. As it can be seen in Table I, the sample containing halloysite is stronger and harder than others. Indeed, at constant strain, the stress is larger in halloysite-containing samples that could be concluded from the steep slope of the stress-strain curves. Thus, halloysite acts as a reinforcing agent and increases bulk modulus.

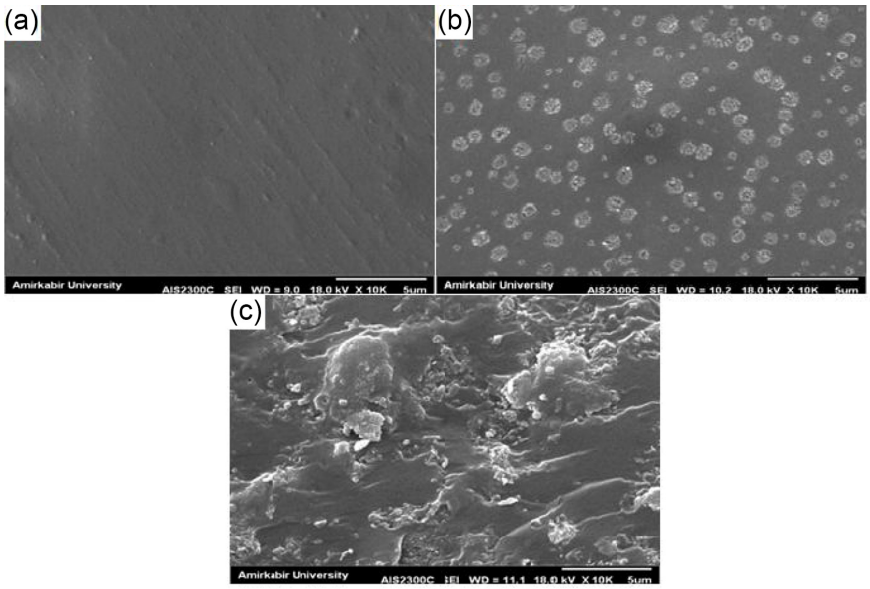

Fig. 6. SEM images of: (a) CA, (b) CA/Cur, and (c) CA/mHNTs/Cur films.

TABLE I
ELASTIC MODULUS, STRAIN STRENGTH, STRESS-AT-BREAK POINT, AND STRAIN-AT-BREAK POINT OF CA, CA/CUR, AND CA/MHNTS/CUR FILMS

Sample	Elastic modulus (MPa)	Strain strength (MPa)	Stress-at-break point (MPa)	Strain-at-break point (%)
CA	0.14±0.06	1.73±0.12	1.14±1.15	41.53±3.13
CA/Cur	0.17±0.35	1.33±0.84	1.78±0.2	7.73±2.12
CA/mHNTs/Cur	0.45±0.20	4.67±0.2	4.9±2.55	19.94±7.24

The halloysite-containing sample is more stable than free-halloysite ones. As in Huang *et al.'s* study, the strain strength of the sample containing CA increases almost 4 times with the addition of mHNT [50]. As expected, the elongation value reduced by adding halloysite, because it is a resistive component and decreases strain-in-break point. The elastic modulus, strain strength, stress-at-break point, and strain-at-break point of CA, CA/Cur, and CA/mHNTs/Cur films have been reported in Table I.

G. In Vitro Curcumin Release

The percentage of drug release versus time is shown in Fig. 7. According to the drug release diagram, the free halloysite sample has a fast release during the first 3 and 4 h and almost 10% release after 96 h. In the sample containing halloysite, drug release has a slow rate due to more stability and adhesive properties created by activating functional groups. It firstly keeps some curcumin and after 96 h has approximately 70% drug release.

In fact, hydroxyl groups are converted to amines and the activity of functional groups in halloysite increases. With the continuation of this stage, the number of available

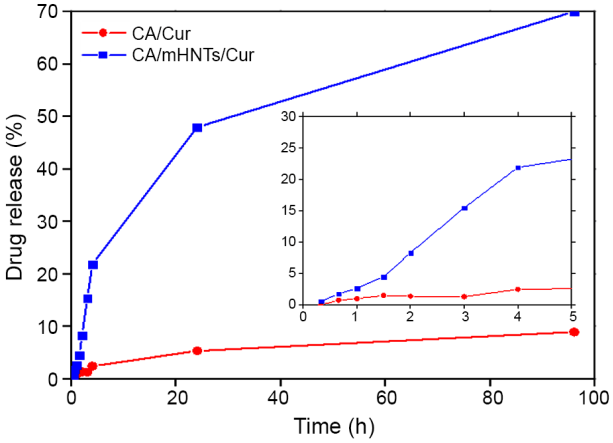

Fig. 7. Drug release of curcumin for CA/Cur and CA/mHNTs/Cur films and the inset exhibits drug release for 5 h.

amine groups and consequently functional groups increases. Adhesion and integrity between nanoparticles and polymer matrix are improved. Consequently, the amount of drug loading is enhanced and a more controllable release will be resulted. It could be concluded that the halloysite-contained sample has a better release rate and halloysite, as a suitable carrier, improves the release rate [29].

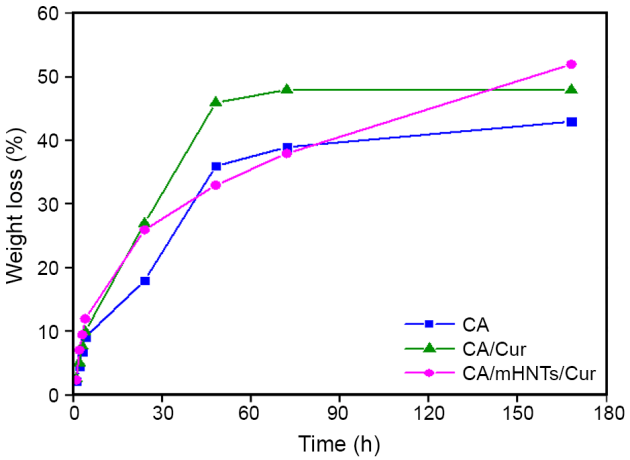

Fig. 8. Degradation rate of CA, CA/Cur, and CA/mHNTs/Cur films.

H. Weight Loss Analysis

The results presented in Fig. 8 implicate that halloysite decreases the rate of degradation. It is due to the excellent adhesion of halloysite to the polymeric matrix and its role as a reinforcing agent receptor and produces a signal for the cells for entering the growth stage or stimulating DNA replication.

I. Cell Adhesion

Halloysite behaves as a positively charged part, and the outer surface of the cell membrane has a negative charge. The electrostatic reaction between the cell and halloysite led to adhesion and round form of the cell [51]. Fig. 9 shows

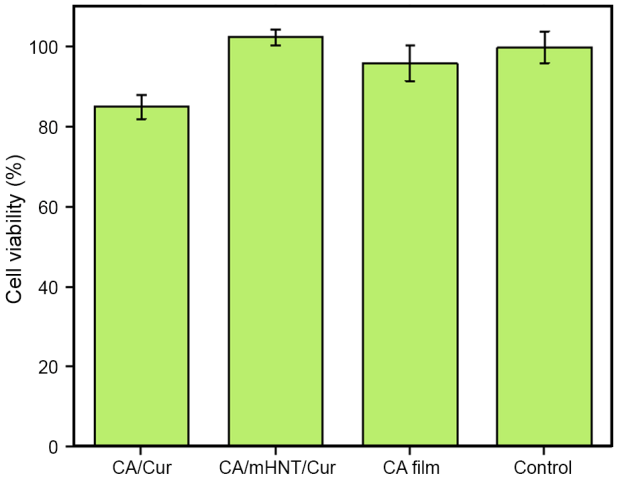

Fig. 10. Column graph of cell viability for CA, CA/Cur, CA/mHNTs/Cur, and control samples.

SEM images of cell adhesion on the CA, CA/Cur, and CA/mHNTs/Cur films after 48 h. The molecules of CA and halloysite can adhere to the extracellular matrix (ECM), integrin receptors or other receptors on the cellular surface in a restricted region. The quick response of these reactions creates cluster integrin.

J. Cell Viability Assay

The cell viability in contact with 48 h sample's extract was investigated by MTT assay. As presented in Fig. 10, the cell viability more than 80% is obtained in the presence of all

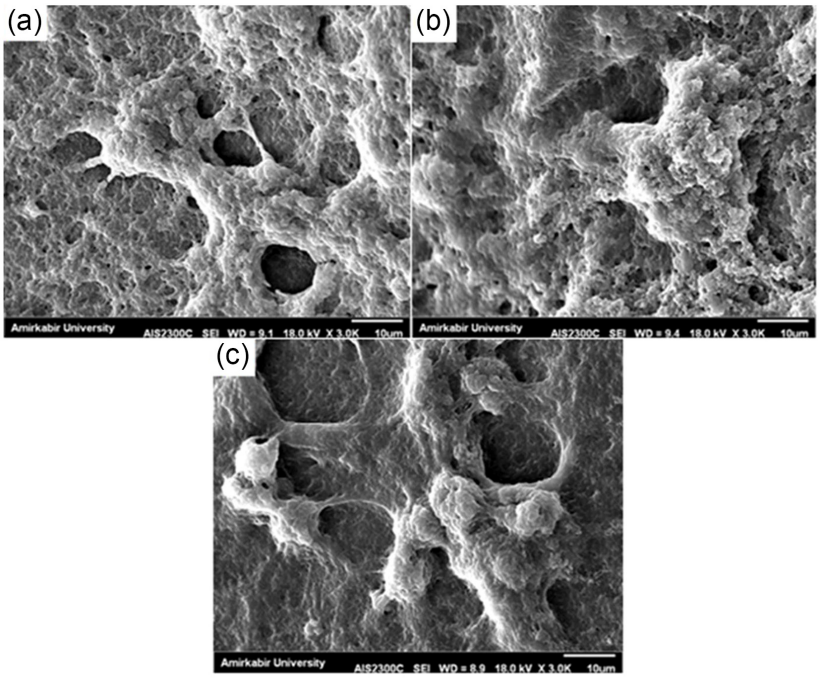

Fig. 9. SEM images of cell adhesion for: (a) CA, (b) CA/Cur, and (c) CA/mHNTs/Cur films.

TABLE II
DIAMETER OF GRAM (+) BACTERIA AND GRAM (-) BACTERIA FOR CA, CA/CUR, AND CA/MHNTS/CUR SAMPLES

Sample	CA (Control) (mm)	CA/Cur (mm)	CA/mHNTs/Cur (mm)
diameter (gram (+) bacteria)	16.54	19.49	20.64
diameter (gram (-) bacteria)	17.89	21.24	27.39

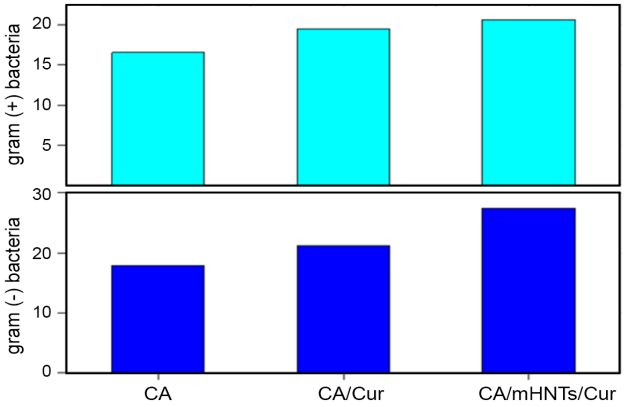

Fig. 11. Column graph of the zone of inhibition diameter for: (a) gram (+) bacteria and (b) gram (-) bacteria for CA, CA/Cur, and CA/mHNTs/Cur samples.

samples extract after passing two days. There is no significant difference in cell viability for CA and CA/mHNTs/Cur films ($p \geq 0.05$), but in the case of CA/Cur sample, it looks that burst release of Cur decreases fibroblast cell viability by about 80% which is still an acceptable percentage [46].

K. Antimicrobial Activity

The results obtained from disk images have shown that there was a zone of inhibition around some disks. This indicates the sensitivity of that bacteria to the disk, and should be reported as sensitive. The disks and halos were investigated under light, and the zone of inhibition diameter was measured by Image J software (Fig. 11 and Table II). It could be obtained from Fig. 11 that CA/mHNTs/Cur and CA/Cur films have higher inhibition zone compared with CA for both gram-positive and gram-negative bacteria. The enhancement in the bacterial activity of CA/mHNTs/Cur rather than CA/Cur sample might be attributed to the mHNTs intrinsic antibacterial properties [52-57]. The addition of curcumin in HNT and CA films and the direct investigation of their properties is the novelty of our study.

IV. CONCLUSION

CA, CA/Cur, and CA/mHNTs/Cur films were prepared by solution casting/solvent evaporation method. FTIR spectra confirmed the presence of CA, Cur, and HNT in the films obtained. Halloysite as additive influences mechanical properties, water vapor transmission rate, and drug release of the samples. Halloysite improves mechanical properties, increases curcumin release and controls the rate of release. This is due to the high activity of Halloysite terminal groups (amine), which retain curcumin for a longer time and prevent eruptive release. After 96 h, the release percentage of the curcumin-containing sample is 70% while it is 10% for the halloysite-free sample in the first 4 h and the next 96 h. The results of the anti-bacterial test show that halloysite-contained film has better properties compared to halloysite-free samples, because of its antibacterial effect. Finally, cell culture and antibacterial tests were performed on the sample in order to examine biologic properties, adhesion rate and cellular morphology of the samples. The results of cell culture assays have shown that all cellulose acetate films are biocompatible, non-toxic, and provide an appropriate substrate for adhesive L929 fibroblast cells. Based on these results, it could be said that the obtained composite is suitable for alternative skin applications. The authors declared no competing financial interest.

REFERENCES

[1] A. Rojas, E. Velásquez, C. Piña, M.J. Galotto, and C.L. de Dicastillo, "Designing active mats based on cellulose acetate/polycaprolactone core/shell structures with different release kinetics", *Carbohyd. Polym.*, vol. 261, no. 117849, pp. 117849, 2021.

[2] O. Suwantong and P. Supaphol, "Applications of Cellulose Acetate Nanofiber Mats", in *Handbook of Polymer Nanocomposites. Processing, Performance and Application*, Springer, 2015, pp. 355-368.

[3] D. Atila, D. Keskin, and A. Tezcaner, "Cellulose acetate based 3-dimensional electrospun scaffolds for skin tissue engineering applications", *Carbohydr. Polym.*, vol. 133, pp. 251-261, 2015.

[4] Y. Luo, S. Wang, M. Shen, R. Qi, Y. Fang, R. Guo, H. Cai, X. Cao, H. Tomás, M. Zhu, and X. Shi, "Carbon nanotube-incorporated multilayered cellulose acetate nanofibers for tissue engineering applications", *Carbohydr. Polym.*, vol. 91, no. 1, pp. 419-427, 2013.

[5] J.C. Chen and K.J. Soden, Anti-adhesion cellulose acetate wound dressing. December 2002.

[6] X. Liu, T. Lin, Y. Gao, Z. Xu, C. Huang, G. Yao, L. Jiang,

Y. Tang, and X. Wang, "Antimicrobial electrospun nanofibers of cellulose acetate and polyester urethane composite for wound dressing", *J. Biomed. Mater. Res. Part B Appl. Biomater.*, vol. 100, no. 6, pp. 1556-1565, 2012.

[7] A.R. Unnithan, G. Gnanasekaran, Y. Sathishkumar, Y.S. Lee, and C.S. Kim, "Electrospun antibacterial polyurethane–cellulose acetate–zein composite mats for wound dressing", *Carbohydr. Polym.*, vol. 102, pp. 884-892, 2014.

[8] C. Huang, S.J. Soenen, E. van Gulck, G. Vanham, J. Rejman, S. Van Calenbergh, C. Vervaet, T. Coenye, H. Verstraelen, M. Temmerman, J. Demeester, and S.C. De Smedt, "Electrospun cellulose acetate phthalate fibers for semen induced anti-HIV vaginal drug delivery", *Biomaterials*, vol. 33, no. 3, pp. 962-969, 2012.

[9] A. Shanbhag, B. Barclay, J. Koziara, and P. Shivanand, "Application of cellulose acetate butyrate-based membrane for osmotic drug delivery", *Cellulose*, vol. 14, no. 1, pp. 65-71, 2007.

[10] S. Tungprapa, I. Jangchud, and P. Supaphol, "Release characteristics of four model drugs from drug-loaded electrospun cellulose acetate fiber mats", *Polymer (Guildf)*, vol. 48, no. 17, pp. 5030-5041, 2007.

[11] Z.Y. Ng, J.Y. Wong, J. Panneerselvam, T. Madheswaran, P. Kumar, V. Pillay, A. Hsu, N. Hansbro, M. Bebawy, P. Wark, P. Hansbro, K. Dua, and D.K. Chellappan, "Assessing the potential of liposomes loaded with curcumin as a therapeutic intervention in asthma", *Colloids Surf. B: Biointerfaces*, vol. 127, no. 1, pp. 51-59, 2018.

[12] S.S. Kamar, D.H. Abdel-Kader, and L.A. Rashed, "Beneficial effect of curcumin nanoparticles-hydrogel on excisional skin wound healing in type-I diabetic rat: histological and immunohistochemical studies", *Ann. Anat.*, vol. 222, pp. 94-102, 2019.

[13] W.Y. Tong, A.Y.K. bin Abdullah, N.A.S. binti Rozman, M.I.A. bin Wahid, Md.S. Hossain, L.C. Ring, Y. Lazim, and W.-N. Tan, "Antimicrobial wound dressing film utilizing cellulose nanocrystal as drug delivery system for curcumin", *Cellulose*, vol. 25, no. 1, pp. 631-638, 2018.

[14] N. Ninan, M. Muthiah, N.A.B. Yahaya, I.-K. Park, A. Elain, T.W. Wong, S. Thomas, and Y. Grohens, "Antibacterial and wound healing analysis of gelatin/zeolite scaffolds", *Colloids Surf. B Biointerfaces*, vol. 115, pp. 244-252, 2014.

[15] C. Aktas, M. Kanter, and Z. Kocak, "Antiapoptotic and proliferative activity of curcumin on ovarian follicles in mice exposed to whole body ionizing radiation", *Toxicol. Ind. Health*, vol. 28, no. 9, pp. 852-863, 2012.

[16] J. Liu, P. Zhu, P. Song, W. Xiong, H. Chen, W. Peng, S. Wang, S. Li, Z. Fu, Y. Wang, and H. Wang, "Pretreatment of adipose derived stem cells with curcumin facilitates myocardial recovery via antiapoptosis and angiogenesis", *Stem Cells Int.*, vol. 2015, 2015. https://doi.org/10.1155/2015/638153

[17] J. Zhao, S. Yu, W. Zheng, G. Feng, G. Luo, L. Wang, and Y. Zhao, "Curcumin improves outcomes and attenuates focal cerebral ischemic injury via antiapoptotic mechanisms in rats", *Neurochem. Res.*, vol. 35, no. 3, pp. 374-379, 2010.

[18] J.D. Altenburg, A.A. Bieberich, C. Terry, K.A. Harvey, J.F. Vanhorn, Z. Xu, V.J. Davisson, and R.A. Siddiqui, "A synergistic antiproliferation effect of curcumin and docosahexaenoic acid in SK-BR-3 breast cancer cells: unique signaling not explained by the effects of either compound alone", *BMC Cancer.*, vol. 11, no. 1, pp. 149, 2011.

[19] M. Shi, Q. Cai, L. Yao, Y. Mao, Y. Ming, and G. Ouyang, "Antiproliferation and apoptosis induced by curcumin in human ovarian cancer cells", *Cell Biol. Int.*, vol. 30, no. 3, pp. 221-226, 2006.

[20] V.R. Yadav, S. Suresh, K. Devi, and S. Yadav, "Effect of cyclodextrin complexation of curcumin on its solubility and antiangiogenic and anti-inflammatory activity in rat colitis model", *Aaps Pharmscitech.*, vol. 10, no. 3, pp. 752, 2009.

[21] J.S. Jurenka, "Anti-inflammatory properties of curcumin, a major constituent of Curcuma longa: a review of preclinical and clinical research", *Altern. Med. Rev.*, vol. 14, no. 2, pp. 141-153, 2009.

[22] S. Ganta, H. Devalapally, and M. Amiji, "Curcumin enhances oral bioavailability and anti-tumor therapeutic efficacy of paclitaxel upon administration in nanoemulsion formulation", *J. Pharm. Sci.*, vol. 99, no. 11, pp. 4630-4641, 2010.

[23] T. Santel, G. Pflug, N.Y.A. Hemdan, A. Schäfer, M. Hollenbach, M. Buchold, A. Hintersdorf, I. Lindner, A. Otto, M. Bigl et al., "Correction: curcumin inhibits glyoxalase 1: a possible link to its anti-inflammatory and anti-tumor activity", *PLoS One*, vol. 6, no. 7, 2011.

[24] J. Trujillo, Y.I. Chirino, E. Molina-Jijón, A.C. Andérica-Romero, E. Tapia, and J. Pedraza-Chaverrí, "Renoprotective effect of the antioxidant curcumin: recent findings", *Redox Biol.*, vol. 1, no. 1, pp. 448-456, 2013.

[25] T. Ak and İ. Gülçin, "Antioxidant and radical scavenging properties of curcumin", *Chem. Biol. Interact.*, vol. 174, no. 1, pp. 27-37, 2008.

[26] R.K. Basniwal, H.S. Buttar, V.K. Jain, and N. Jain, "Curcumin nanoparticles: preparation, characterization,

and antimicrobial study", *J. Agric. Food Chem.*, vol. 59, no. 5, pp. 2056-2061, 2011.

[27] M. Pisano, G. Pagnan, M.A. Dettori, S. Cossu, I. Caffa, I. Sassu, L. Emionite, D. Fabbri, M. Cilli, F. Pastorino, G. Palmieri, G. Delogu, M. Ponzoni, and C. Rozzo, "Enhanced anti-tumor activity of a new curcumin-related compound against melanoma and neuroblastoma cells", *Mol. Cancer.*, vol. 9, no. 1, pp. 137, 2010.

[28] O. VSuwantong, P. Opanasopit, U. Ruktanonchai, and P. Supaphol, "Electrospun cellulose acetate fiber mats containing curcumin and release characteristic of the herbal substance", *Polymer (Guildf)*, vol. 48, no. 26, pp. 7546-7557, 2007.

[29] T.S. Saranya, V.K. Rajan, R. Biswas, R. Jayakumar, S. Sathianarayanan, "Synthesis, characterisation and biomedical applications of curcumin conjugated chitosan microspheres", *Int. J. Biol. Macromol.*, vol. 110, pp. 227-233, 2017.

[30] G. Cavallaro, G. Lazzara, M. Massaro, S. Milioto, et al., "Biocompatible poly(N-isopropylacrylamide)-halloysite nanotubes for thermoresponsive curcumin release", *J. Phys. Chem. C*, vol. 119, no. 16, pp. 8944-8951, 2015.

[31] F. Shahamati Fard, S. Akbari, E. Pajootan, and M. Arami, "Enhanced acidic dye adsorption onto the dendrimer-based modified halloysite nanotubes", *Desalin. Water Treat.*, vol. 57, no. 54, pp. 26222-26239, 2016.

[32] M. Shahbaz Arshad, M. Qaiser, K. Mahmood, M. Harris Shoaib, N. Ameer, N. Ramzan et al., "Chitosan/halloysite nanotubes microcomposites: a double header approach for sustained release of ciprofloxacin and its hemostatic effects", *Int. J. Biol. Macromol.*, vol. 212, pp. 314-23, 2022.

[33] A. Mohebali and M. Abdouss, "Layered biocompatible pH-responsive antibacterial composite film based on HNT/PLGA/chitosan for controlled release of minocycline as burn wound dressing", *Int. J. Biol. Macromol.*, vol. 164, no. 1, pp. 4193-204, 2020.

[34] N.P. Risyon, S.H. Othman, R. Kadir Basha, and R.A. Talib, "Characterization of polylactic acid/halloysite nanotubes bionanocomposite films for food packaging", *Food Packag. Shelf Life*, vol. 23, pp. 100450, 2020.

[35] I. Anastopoulos, A. Mittal, M. Usman, J. Mittal, G.H. Yu, A. Nunez-Delgado, and M. Usmancd, "A review on halloysite-based adsorbents to remove pollutants in water and wastewater", *J. Mol. Liq.*, vol. 269, pp. 855-868, 2018.

[36] K. Jeamjumnunja, O. Cheycharoen, N. Phongzitthiganna, S. Hannongbua, and C. Prasittichai, "Surface-modified halloysite nanotubes as electrochemical CO_2 sensors", vol. 4, no. 4, pp. 3686-3695, 2021.

[37] B. Huang, M. Liu, and C. Zhou, "Cellulose–halloysite nanotube composite hydrogels for curcumin delivery", *Cellulose*, vol. 24, no. 7, pp. 2861-2875, 2017.

[38] C. Dionisi, N. Hanafy, C. Nobile, M.L. De Giorgi, R. Rinaldi, S. Casciaro, Y.M. Lvov, and S. Leporatti, "Halloysite clay nanotubes as carriers for curcumin: characterization and application", *IEEE Trans Nanotechnol.*, vol. 15, no. 5, pp. 720-724, 2016.

[39] M.K. Pierchala, M. Makaremi, H.L. Tan, M. Malgorzata, J. Pushpamalar, S. Muniyandy, A. Solouk, S.M. Lee, and P. Pasbakhsh, "Nanotubes in nanofibers: antibacterial multilayered polylactic acid/halloysite/gentamicin membranes for bone regeneration application", *Appl. Clay. Sci.*, vol. 160, pp. 95-105, 2017.

[40] P. Dramou, M. Fizir, A. Taleb, A. Itatahine, N. Sintali Dahiru, Y.A. Mehdi, L. Wei, J. Zhang, and H. He, "Folic acid-conjugated chitosan oligosaccharide-magnetic halloysite nanotubes as a delivery system for camptothecin", *Carbohydr. Polym.*, vol. 197, pp. 117-127, 2018.

[41] P. Yuan, P.D. Southon, Z. Liu, and J.M. Hook, "Functionalization of halloysite clay nanotubes by grafting with γ-aminopropyltriethoxysilane", *J. Phys. Chem. C*, vol. 112, no. 40, pp. 15742-15751, 2008.

[42] G. Zeng, Y. He, Y. Zhan, L. Zhang, Y. Pan, C. Zhang, and Z. Yu, "Novel polyvinylidene fluoride nanofiltration membrane blended with functionalized halloysite nanotubes for dye and heavy metal ions removal", *J. Hazard Mater.*, vol. 317, pp. 60-72, 2016.

[43] Y.-F. Shi, Z. Tian, Y. Zhang, H.-B. Shen, and N.-Q. Jia, "Functionalized halloysite nanotube-based carrier for intracellular delivery of antisense oligonucleotides", *Nanoscale Res Lett.*, vol. 6, no. 1, pp. 608, 2011.

[44] F.J. Shariatzadeh, S. Nour, D. Sadeghi, and A. Solouk, Evaluation of physical properties of semi-thickness skin, acellular dermis and fascia as biologic skin substitutes. In: Biomedical Engineering and 2016 1st International Iranian Conference on Biomedical Engineering (ICBME), 2016 23rd Iranian Conference on. IEEE; 2016:1-6.

[45] S. Bonakdar, S.H. Emami, M.A. Shokrgozar, A. Farhadi, S.A.H. Ahmadi, and A. Amanzadeh, "Preparation and characterization of polyvinyl alcohol hydrogels crosslinked by biodegradable polyurethane for tissue engineering of cartilage", *Mater. Sci. Eng.*, vol. 30, no. 4, pp. 636-643, 2010.

[46] S.S. Zargarian, V. Haddadi-Asl, and H. Hematpourh,

"Carboxylic acid functionalization of halloysite nanotubes for sustained release of diphenhydramine hydrochloride", *J. Nanopart. Res.*, vol. 17, no. 5, pp. 218, 2015.

[47] M. Delyanee, A. Solouk, S. Akbari, and E. Seyedjafari, "Modification of electrospun poly(l-lactic acid)/ polyethylenimine nanofibrous scaffolds for biomedical application", *Int. J. Polym. Mater. Polym. Biomater.*, vol. 67, no. 4, pp. 247-257, 2018.

[48] S.M. Saeed, H. Mirzadeh, M. Zandi, and J. Barzin, "Designing and fabrication of curcumin loaded PCL/ PVA multi-layer nanofibrous electrospun structures as active wound dressing", *Prog. Biomater.*, vol. 6, no. 1-2, pp. 39-48, 2017.

[49] P. Owlia, L. Sadeghzadeh, F. Orang, M. Rafienia, and S. Bonakdar, "Evaluation of ceftriaxone releasing from microspheres based on starch against Salmonella spp", *Biotechnology*, vol. 6, no. 4, pp. 597-600, 2007.

[50] B. Huang, M. Liu, and C. Zhou, "Cellulose–halloysite nanotube composite hydrogels for curcumin delivery", *Cellulose*, vol. 24, pp. 2861-2875, 2017.

[51] M. Rafienia, B. Zarinmehr, S.A. Poursamar, S. Bonakdar, M. Ghavami, and M. Janmaleki, "Coated urinary catheter by PEG/PVA/gentamicin with drug delivery capability against hospital infection", *Iran Polym. J.*, vol. 22, no. 2, pp. 75-83, 2013

[52] S. Bordeepong, D. Bhongsuwan, T. Pungrassami, and T. Bhongsuwan, "Characterization of halloysite from Thung Yai District, Nakhon Si Thammarat Province, in Southern Thailand", *Songklanakarin J. Sci. Technol.*, vol. 33, no. 5, 2011.

[53] E.G. Bediako, E. Nyankson, D. Dodoo-Arhin, B. Agyei-Tuffour, D. Łukowiec, B. Tomiczek, A. Yaya, and J.K. Efavi, "Modified halloysite nanoclay as a vehicle for sustained drug delivery", *Heliyon*, vol. 4, no. 7, pp. e00689, 2018.

[54] J. Kurczewska, M. Cegłowski, B. Messyasz, and G. Schroeder, "Dendrimer-functionalized halloysite nanotubes for effective drug delivery", *Appl. Clay Sci.*, vol. 153, pp. 134-143, 2018.

[55] M. Delyanee, A. Solouk, S. Akbari, and M. Daliri Joupari, "Engineered hemostatic bionanocomposite of poly(lactic acid) electrospun mat and amino-modified halloysite for potential application in wound healing", *Polym. Adv. Technol.*, Wiley Online Library, 2021. https://doi.org/10.1002/pat.5399

[56] N.T. Ardekani, M. Khorram, K. Zomorodian, S. Yazdanpanah, and H. Veisi, "Evaluation of electrospun poly(vinyl alcohol)-based nanofiber mats incorporated with Zataria multiflora essential oil as potential wound dressing", *Int. J. Biol. Macromol.*, vol. 125, pp. 743-750, 2019.

[57] V. Vivcharenko and A. Przekora, "Modifications of wound dressings with bioactive agents to achieve improved pro-healing properties", *Appl. Sci.*, vol. 11, no. 9, pp. 4114, 2021.